Cellular and Molecular Life Sciences (2021) 78:695–713
https://doi.org/10.1007/s00018-020-03533-8

ORIGINAL ARTICLE

Dissecting the initiation of female meiosis in the mouse at single-cell resolution

Wei Ge[1] · Jun-Jie Wang[1] · Rui-Qian Zhang[1] · Shao-Jing Tan[1] · Fa-Li Zhang[1] · Wen-Xiang Liu[1] · Lan Li[1] · Xiao-Feng Sun[1] · Shun-Feng Cheng[1] · Paul W. Dyce[2] · Massimo De Felici[3] · Wei Shen[1]

Received: 19 December 2019 / Revised: 22 March 2020 / Accepted: 17 April 2020 / Published online: 4 May 2020

Abstract

Meiosis is one of the most finely orchestrated events during gametogenesis with distinct developmental patterns in males and females. However, the molecular mechanisms involved in this process remain not well known. Here, we report detailed transcriptome analyses of cell populations present in the mouse female gonadal ridges (E11.5) and the embryonic ovaries from E12.5 to E14.5 using single-cell RNA sequencing (scRNA seq). These periods correspond with the initiation and progression of meiosis throughout the first stage of prophase I. We identified 13 transcriptionally distinct cell populations and 7 transcriptionally distinct germ cell subclusters that correspond to mitotic (3 clusters) and meiotic (4 clusters) germ cells. By analysing cluster-specific gene expression profiles, we found four cell clusters correspond to different cell stages en route to meiosis and characterized their detailed transcriptome dynamics. Our scRNA seq analysis here represents a new important resource for deciphering the molecular pathways driving female meiosis initiation.

Keywords Single-cell RNA seq · Meiosis initiation · Female germ cells

Abbreviations

PGCs	Primordial germ cells
RA	Retinoic acid
BMP	Bone morphogenetic protein
scRNA	Single-cell RNA sequencing
tSNE	t-Distributed Stochastic Neighbor Embedding
DEGs	Differentially expressed genes
GO	Gene ontology
PCA	Principal component analysis
GRNs	Gene regulatory networks
SCENIC	Single-cell regulatory network inference and clustering
ES	Embryonic stem
GEMs	Gel-bead in emulsions

Electronic supplementary material The online version of this article (https://doi.org/10.1007/s00018-020-03533-8) contains supplementary material, which is available to authorized users.

✉ Wei Shen
wshen@qau.edu.cn; shenwei427@163.com

[1] College of Life Sciences, Qingdao Agricultural University, Qingdao 266109, China

[2] Department of Animal Sciences, Auburn University, Auburn, AL 36849, USA

[3] Department of Biomedicine and Prevention, University of Rome Tor Vergata, 00133 Rome, Italy

Introduction

In mammals, the primordial germ cells (PGCs) are considered germline stem cells that give rise to the male and female gametes, ultimately responsible for the survival of species and the transmission of genetic information across generations [1], of which meiosis is one of the most important processes. Meiosis in female mammals begins in the developing ovaries during the embryonic/fetal period, and is arrested at the end of prophase I around or just after birth [2]. In mice, female PGCs colonize the gonadal ridges from E10.5 to E12.5 and after some rounds of mitotic division begin to enter meiosis between E13.5 and E14.5 [3, 4]. During the mitosis–meiosis transition, germ cells undergo extensive changes in gene expression as they progress through the leptotene, zygotene, pachytene and diplotene stages until arrested at the dictyate stage of meiosis prophase I [5]. Meiosis initiation has long been considered as the gatekeeper of successful gametogenesis [6]. In fact, the fidelity of meiosis initiation along with progression is vital for future reproductive health and defects in such processes

can lead to reproductive diseases including premature ovarian failure, polycystic ovary syndrome and even infertility [5, 7]. However, in mammals, due to the paucity of information regarding the molecular mechanisms regulating the initiation and progression of meiosis, the aetiology of such reproductive diseases remains elusive. To obtain insights into these processes, researchers have used a variety of experimental approaches. For example, in the mouse, many attempts have been performed using the in vitro culture of embryonic gonads and isolated PGCs, and more recently, producing gametes from various stem cell types to reproduce meiotic entry and progression has been achieved [6, 8]. For obvious reasons, this latter approach is particularly useful in humans where promising results have been very recently obtained [9]. Several studies have reported the successful generation of germ cell-like cells from stem cells, however, until recently convincing evidence that such cells were able to correctly enter meiosis were lacking [10–12]. In 2016, Zhou's group and Hayashi's group, reported the successful derivation of functional sperm and oocytes from pluripotent stem cells, respectively [13, 14]. Although these studies provide valuable sources for investigating mammalian meiosis under complete in vitro conditions, the germ cell differentiation efficiency was limited, and many germ cells showed abnormal meiotic entry as evidenced by the increased percentage of asynapsis in comparison to endogenous and in vitro cultured germ cells.

After many decades of work identifying compounds able to induce PGC formation in females or inhibit male PGC entry into meiosis, a retinoic acid (RA)-*Stra8* signaling pathway has emerged as a key regulator of meiosis initiation in mice [15, 16]. Today, it is widely accepted that in mammals, RA secreted from the mesonephroi activates meiotic gene expression (i.e., *Sycp3*, *Sycp1*, *Stra8* and *Rec8*) and initiates meiotic programs in female PGCs [15]. However, recent studies from Miyauchi et al. in accord with previous results by Farini et al. found that RA alone is not sufficient to initiate meiosis onset in PGC-like cells produced from stem cells in vitro and demonstrated that the crosstalk between RA signalling and bone morphogenetic protein (BMP) signalling is pivotal for the activation of meiotic transcriptional cascades [17, 18]. Besides, it is also worth noting that previous studies mainly focused on gene expression dynamics during germ cell fate commitment and meiosis initiation, while key regulators of meiotic progression remain to be identified [19–21].

In the present study, by using high-throughput single-cell RNA sequencing (scRNA seq), we analysed the transcriptome data from 19,387 individual cells that were obtained from gonadal ridges and ovaries of E11.5–E14.5 mouse embryos. Based on these data, we successfully identified germ cell and somatic cell subpopulations; furthermore, we characterized detailed germ cell transcriptome gene expression signatures en route to meiosis. Pseudo-time ordering analysis successfully recapitulated germ cell meiosis initiation trajectory and revealed key molecular events involved during the transition from mitosis to meiosis. We also discussed the heterogeneity of the ovarian somatic cells. The results obtained here provide novel information and insights into the initiation and progression of meiosis and the diversity of somatic cells and lineages within the developing gonads.

Materials and methods

Animals

All mice used in this study were C57/BL6 mice purchased from Beijing Vital River Laboratory Animal Technology Co., Ltd. Experimental procedures involved in this study were approved by the Animal Care and Use Committee of Qingdao Agricultural University. Briefly, all C57/BL6 mice were housed in a light and temperature-controlled room (light: 12 h dark and 12 h light cycles; temperature: 24 ± 0.5 °C) with ad libitum access to food and water. Then, 6-week-old female mice were mated with 8-week-old male mice (3:1) overnight and the vaginal plug was checked the next morning. Mice with a vaginal plug were considered 0.5 days post coitum (dpc).

In vitro isolation of genital ridges and sex genotyping

Pregnant mice were killed by cervical dislocation and the genital ridges of the foetus were isolated using a pair of precise forceps as previously described [22]. For the characterization of E11.5 foetal ovarian tissues, the *Sry* and *Ube1* genes were used for sexing. The following primers were used according to the previously described procedure: *Sry*: F: 5′-CTG TGT AGG ATC TTC AAT CTC T-3′; R: 5′-GTG GTG AGA GGC ACA AGT TGG C-3′ and *Ube1*: F: 5′-TGG TCT GGA CCC AAA CGC TGT CCA CA-3′; R: 5′-GGC AGC AGC CAT CAC ATA ATC CAG ATG-3′ [23]. Briefly, a small piece of skin tissue of each foetus was isolated and was boiled in water for 10 min; then the tissues were directly used as PCR templates and PCR was performed using 2 × EasyTag PCR SuperMix (Transgene, Beijing, China, AT311-03) according to the manufacturer's instructions. The obtained PCR products were then electrophoresed on a 2% agarose gel (TSINGKE, Beijing, China, R9012LE) at 100 V for 30 min (*Sry*) or 1 h (*Ube1*). *Gapdh* (F primer: 5′-AGG TCG GTG TGA ACG GAT TTG-3′; R primer: 5′-TGT AGA CCA TGT AGT TGA GGT CA-3′) was used as a loading control. For sex determination of E12.5, E13.5 and E14.5 genital ridges, the sex was morphologically

distinguishable according to the formation of testis cords in the male gonads [24].

Meiotic chromosome spreads staining assay

Immunofluorescence staining of meiotic chromosome spreads was used for determining the meiotic progression of germ cells at different stages as we previously described [25, 26]. Briefly, the isolated genital ridges were incubated with hypotonic solution (30 mM Tris, 50 mM sucrose, 17 mM citric acid, 5 mM EDTA, 2.5 mM DL-dithiothreitol and 1 mM phenylmethanesulfonyl fluoride in water) for 30 min at room temperature. After that, the genital ridges were transferred into 4% paraformaldehyde solution (Solarbio, Beijing, China, P1110) and the ovarian tissues were mechanically separated. The suspended ovarian cells were then spread onto glass slides overnight. The next morning, the slides were washed with 0.04% Photo-Flo 200 (Kodak, Rochester, NY, USA, 146 4502) and then blocked with PBS supplemented with 1% goat serum (BOSTER, Wuhan, China, AR0009) and 0.05 M Tris–HCl. After blocking, the first antibody (SYCP3, Novus Littleton, CO, USA, NB300-232; γH2AX, Abcam, Shanghai, China, ab26350) was then added and the slides were incubated at 37 °C for 8 h. After three washes to remove unconjugated antibodies, the secondary antibodies (Donkey anti-Rabbit IgG H&L Alexa Fluor® 555, Abcam, ab150074; Goat anti-Mouse IgG H&L Alexa Fluor® 488, Abcam, ab150113) were then incubated at 37 °C for 2 h and the slides were mounted with Vectashield mounting media (Vector Laboratories, Burlingame, CA, USA, H-1000). All pictures were taken using a Leica Laser Scanning Confocal Microscope imaging system (Leica TCS SP5 II, Wetzlar, Germany).

Immunofluorescence analysis and fluorescence intensity analysis

The isolated single-cell pellets were first fixed with 4% paraformaldehyde at 4 °C for 30 min; then, the cell pellets were plated on 3-aminopropyl-triethoxysilane (APES, ZSbio, Beijing, China, ZLI-9001) treated slides. Permeabilization was performed with PBST solution consisting of PBS supplemented with 0.5% Triton X-100 (Solarbio, Beijing, China, T8200) for 10 min at room temperature. After permeabilization, slides were blocked with PBST supplemented with 10% goat blocking serum (BOSTER, AR0009) for 45 min at room temperature. Primary antibodies (DDX4/MVH, Abcam, ab27591; UTF1, Abcam, ab24273; ETV5, Abcam, ab102010; NR3C1, Abcam, ab2768) were diluted in blocking buffer and were incubated with the slides at 4 °C overnight. In the next morning, the slides were washed three times with PBS supplemented with 1% BSA, and then the secondary antibodies were added and were incubated with the slides at 37 °C for 2 h. Finally, the slides were mounted with Vectashield mounting media and pictures were taken using a Leica Laser Scanning Confocal Microscope imaging system. The fluorescence intensity analysis was analysed with ImageJ software (v 1.48, National Institutes of Health, Bethesda, MD, USA) according to the manufacturer's instructions.

Western blot analysis

Western blot analysis procedure was performed as we previously described [27]. Briefly, after isolation of genital ridges, the samples were mixed and then total proteins were extracted with RIPA lysis solution (Beyotime, Haimen, China, P0013C) on ice for 30 min. Electrophoresis was performed with 4–10% sodium dodecyl sulphate (Solarbio, S8010) and the target proteins were then transferred to nitrocellulose membranes (Millipore, Bedford, MA, USA). Primary antibodies (STK31, Abcam, ab155172; GAPDH, Immunoway, Newark, DE, USA, YM3040) were incubated with the membranes at 4 °C overnight after blocking, and secondary antibodies (Horseradish peroxidase (HRP)-conjugated goat anti-rabbit or mouse IgG secondary antibodies, Beyotime, A0208 and A0216) were incubated at room temperature for 1 h. Chemiluminescence was performed with BeyoECL Plus kit (Beyotime, P0018) and pictures were taken with chemiluminescence (ECL) detection system (ProteinSimple, San Jose, CA, USA).

Single-cell library preparation and sequencing

Single-cell library was prepared using the 10 × Genomics Chromium Single Cell 3′ Library and Gel Bead Kit v2 (10 × Genomics, Pleasanton, CA, USA, 120237) according to the manufacturer's instructions. Briefly, to obtain the desired number of cells from genital ridges, about 8–10 female foetuses were prepared for each group. The genital ridges were then mixed and dissociated with a 0.25% trypsin–EDTA solution for 3 min at 37 °C. After trypsinization, the cell suspension was filtered with a 40-μm cell strainer (BD Biosciences, San Jose, CA, USA, 352340) and was washed three times with PBS solution supplemented with 0.04% bovine serum albumin (BSA, Sigma, St. Louis, MO, USA, A1933). To determine whether the cells obtained were eligible (cell viability > 80%, cell concentrations = 1000 cells/μl) for downstream analysis, the cell viability was evaluated using trypan blue staining with a haemocytometer (Bio-Rad, Hercules, CA, USA, TC20) and the cell concentration was adjusted to 1000 cells/μl before loading to the single-cell chip. The Gel-Bead in Emulsions (GEMs) were then generated with Chromium 10 × Single Cell System (10 × Genomics). To barcode cDNA in each cell, the cells were then lysed and followed by a reverse

transcription procedure. After that, cDNA recovery was performed using DynaBeads MyOne Silane Beads (Invitrogen, Carlsbad, CA, USA, 37002D) according to the manufacturer's instructions. cDNA libraries were then prepared using 10 × Genomics Chromium Single Cell 3′ Library and Gel Bead Kit v2 following the manufacturer's guide and sequencing was performed with an Illumina HiSeq X Ten sequencer (Illumina, San Diego, CA, USA) with pair-end 150 bp (PE150) reads.

Single sample analysis and aggregation

CellRanger v2.2.0 software (https://www.10xgenomics.com/) was used to analyse the obtained datasets with '–force-cells = 5000' argument to obtain the same number of cells for downstream analysis. The 10 × Genomics pre-built mouse genome for mm10-3.0.0 (https://support.10xgenomics.com/single-cell-gene-expression/software/downloads/latest) was used as the reference genome. After the CellRanger pipeline, the gene-barcode matrices were then analysed with Seurat single-cell RNA seq analysis R package (v3.0) [28]. The analysis procedure was performed according to the package's user guide with little modifications. Briefly, cells with minimal genes less than 200 and genes expressed in less than 3 cells were removed to keep high-quality datasets for downstream analysis. After normalization, the four datasets were then merged with the Seurat RunMultiCCA function. To characterize cell clusters, they were visualized with Seurat RunTSNE function based on the t-distributed Stochastic Neighbor Embedding (tSNE) algorithm with default settings and cell clusters were calculated with FindClusters function at a resolution of 0.6. To characterize cell cluster markers the Seurat FindAllMarkers function was used.

Subclustering, gene ontology and protein–protein network enrichment analysis

After the characterization of all cell clusters in genital ridges, cell clusters were further divided into different groups according to their cell identity. To extract the same type of cells for downstream analysis, we used SubsetData function implemented in Seurat package to extract germ cell and somatic cell subclusters. The extracted subclusters were then reanalysed with the single Seurat analysis procedure to gain further insight into the subcluster information of particular cell types. After clustering and subclustering, cluster-specific markers were obtained with the FindAllMarkers function. To identify the intergenic relationship within clusters, we selected the cluster-specific top 500 differentially expressed genes based on p value and performed Gene Ontology (GO) analysis using Metascape (http://metascape.org). To infer protein–protein network from different gene sets, STRING database (https://string-db.org/) was used to infer protein–protein interaction network and the network was further visualized with Cytoscape software (v3.7.0, https://cytoscape.org/).

Single-cell pseudo-time trajectory analysis

Single-cell pseudo-time trajectory analysis was performed using R package Monocle 2 (v2.8.0) according to the online tutorials (http://cole-trapnell-lab.github.io/monocle-release/tutorials/) [29, 30]. Briefly, Monocle object was directly constructed using Monocle implemented new Cell Data Set function from Seurat object with lower detection limit = 0.5 and we used the Seurat-determined variable genes as highly variable genes for ordering. Dimensionality was reduced using the DDRTree method with regression based on the number of UMIs. The root state was chosen according to their Seurat cell identity information and branch-specific gene expression was calculated using Monocle implemented BEAM function and branched heatmap was further visualized by "plot_genes_branched_heatmap" function.

Single-cell regulatory network inference and clustering

To reveal gene regulatory networks during germ cell meiosis initiation, we performed regulatory network inference and clustering based on SCENIC, a modified method for inferring gene regulatory networks from single-cell RNA seq data [31]. The SCENIC analysis was performed according to the SCENIC online tutorial (https://github.com/aertslab/SCENIC). First, we extracted the single-cell RNA-seq expression matrix from Seurat, in which each column represents a cell ID and each row represents a gene; then we used geneFiltering function to remove genes with UMI counts across all samples less than 80.12 and expressed in less than 1% of cells. After that, we used GENIE3 to infer co-expression matrix which contains potential regulators. To identify potential direct-binding targets, RcisTarget was then used based on DNA-motif analysis and we used databases (mm10) that score the motifs in the promoter of the genes (up to 500 bp upstream the TSS), and in the 10-kb around the TSS (± 10 kb). Last, we used the AUCell algorithm to calculate regulon activity in each cell and convert the network activity into ON/OFF (binary activity matrix) with default settings.

Data availability

The sequencing raw data have been deposited in NCBI's Gene Expression Omnibus (GEO) under accession number: GSE128553.

Results

Identification and characterization of the ovarian cell populations

To decipher the gene expression landscape and dissect the cellular heterogeneity during the initiation of meiosis in female germ cells, we dissociated ovarian tissues from E11.5, E12.5, E13.5, and E14.5 murine embryos and prepared single-cell suspensions for scRNA seq (Fig. 1a and Supplementary Fig. 1a, b) [32, 33]. To verify the *bona fide* progression of meiosis, we performed ovarian tissue cytospreads for SYCP3 and γH2AX to characterize the meiotic stage (Fig. 1b) [25] and calculated the percentage of meiotic cells (SYCP3 positive oocytes) at each time point (Fig. 1c). Consistent with previous findings, germ cells in E11.5 and E12.5 were mitotic, and it was not until E13.5 that some germ cells entered meiosis [34].

After filtering low-quality cells based on the number of genes, unique molecular identifiers and the percentage of mitochondria genes (Supplementary Fig. 1c), we obtained a total of 19,387 ovarian cells (4916 cells for E11.5, 4842 cells for E12.5, 4842 cells for E13.5, and 4787 cells for E14.5, respectively) and 19,321 genes, with the median genes per cell ranging from 3097 to 3613 (Supplementary Fig. 1a). To characterize cell identity, we integrated the four samples and performed t-distributed Stochastic Neighbor Embedding (tSNE) clustering analysis to dissect cellular heterogeneity among the ovarian cell populations (Fig. 1d). After the tSNE projection, the four datasets integrated according to Seurat-recommended algorithm (Supplementary Fig. 1d). Further analysis delineated 13 transcriptionally distinct cell clusters across the four time points (Fig. 1d). To identify germ cell populations within the plot, we visualized two genes that serve as classical germ cell markers, *Dazl* and *Ddx4* [35, 36]. Their expression across all single cells was determined and it was found that three cell clusters highly expressed the germ cell marker genes (Fig. 1e). Pregranulosa cells or their precursors (supporting somatic cells) were identified within three distinct clusters on the basis of the elevated expression of *Wnt4* and *Wnt6* (Supplementary Fig. 1e) [37, 38]. We also identified five somatic cell clusters with their classic makers including mesothelial cells (*Lhx9* and *Upk3b*) [39, 40], interstitial cells (*Col1a2* and *Bgn*) [41], endothelial cells (*Pecam1* and *Kdr*) [42, 43] and two contaminative somatic cell populations from blood, immune cells (*Cd52* and *Car2*) and erythroid cells (*Alas2* and *Alad*) [44, 45] (Supplementary Fig. 1e). Together, these data provided evidence of the heterogeneity of all somatic cell populations during the time frame analysed.

After this initial cluster identification, we began to analyse the dynamics of each cell population, principally of the germ cells and pregranulosa cells. To deconstruct the heterogeneous composition of the three germ cell clusters in the tSNE plot, we visualized the expression of the early PGC marker genes (*Pou5f1*, *Sox2*, *Utf1* and *Sall4*) [46, 47], and the meiotic related genes (early: *Stra8*, *Sycp3* and *Rec8*; late: *Sycp1*, *Tex14* and *Mael*) (Fig. 1e and Supplementary Fig. 1e) [48–50]. These sets of genes showed distinct expression patterns: early PGC markers were mainly expressed in the lower part of clusters while the meiotic-related genes were found mainly in the upper region. On this basis, we allocated premeiotic PGCs, along with early and late meiotic germ cells within the three germ cell clusters (Fig. 1d). For the pregranulosa cell population, due to the lack of markers distinguishing supporting and pregranulosa cells, we interpreted such identities by combining the three *Wnt4* and *Wnt6* positive clusters with those of Supplementary Fig. 1d. In particular, since in the mouse the majority of supporting cells differentiate into pregranulosa cells after gonadal sex determination [37], we identified the supporting cell cluster representing the highest percentage of cells in the E11.5–E12.5 gonads along with two pregranulosa cell populations mainly in E13.5–E14.5 ovaries (Fig. 1d). These analyses together with the calculation of the percentage of the cells within each cluster (Supplementary Fig. 2a), preliminarily delineated the beginning and progression of meiosis in germ cells and the dynamics of the ovarian cell lineages.

To gain in-depth insight into the cluster-specific gene signatures and the functional gene categories of the ovarian cell populations, we also analysed cell cluster-specific gene expression in more detail (Fig. 1f and Supplementary Fig. 2b). As expected, genes related to pluripotency, like *Pou5f1*, *Sox2* and *Utf1*, showed high expression in the early premeiotic PGCs that gradually decreased with the beginning and progression of meiosis. Conversely, the expression of meiotic genes such as *Stra8*, *Sycp1* and *Sycp3* significantly increased with the progression of meiosis (Fig. 1f and Supplementary Fig. 2c). To further validate our Seurat-identified signature genes, we also performed immunofluorescence analysis on Seurat-identified mitotic marker expression UTF1, which also showed similar results (Supplementary Fig. 2d).

In total, we found 634, 654 and 1189 differentially expressed genes (DEGs) in mitotic, early and late meiotic germ cells, respectively (Supplementary Table 1). Interestingly, gene ontology (GO) analysis of mitotic germ cells mainly enriched in pluripotent and cell cycle-related genes such as *Dppa5a*, *Utf1*, *Cenpf* and *Ifitm3*, and enriched GO terms of "cell division", "ribonucleoprotein complex biogenesis" and "regulation of DNA metabolic process". This supports the notion of active PGC proliferation prior to the mitosis to meiosis transition [51]. Early meiotic germ cells were enriched in *Stra8*, *Dazl*, *Smc1b*, *Hells* and *Sycp1*, while late meiotic germ cells enriched in *Smc1b*, *Sycp3*, *Sycp1*, *Tex101* and *Tex15*. Noteworthy, both early meiotic germ cells and late meiotic germ cells enriched

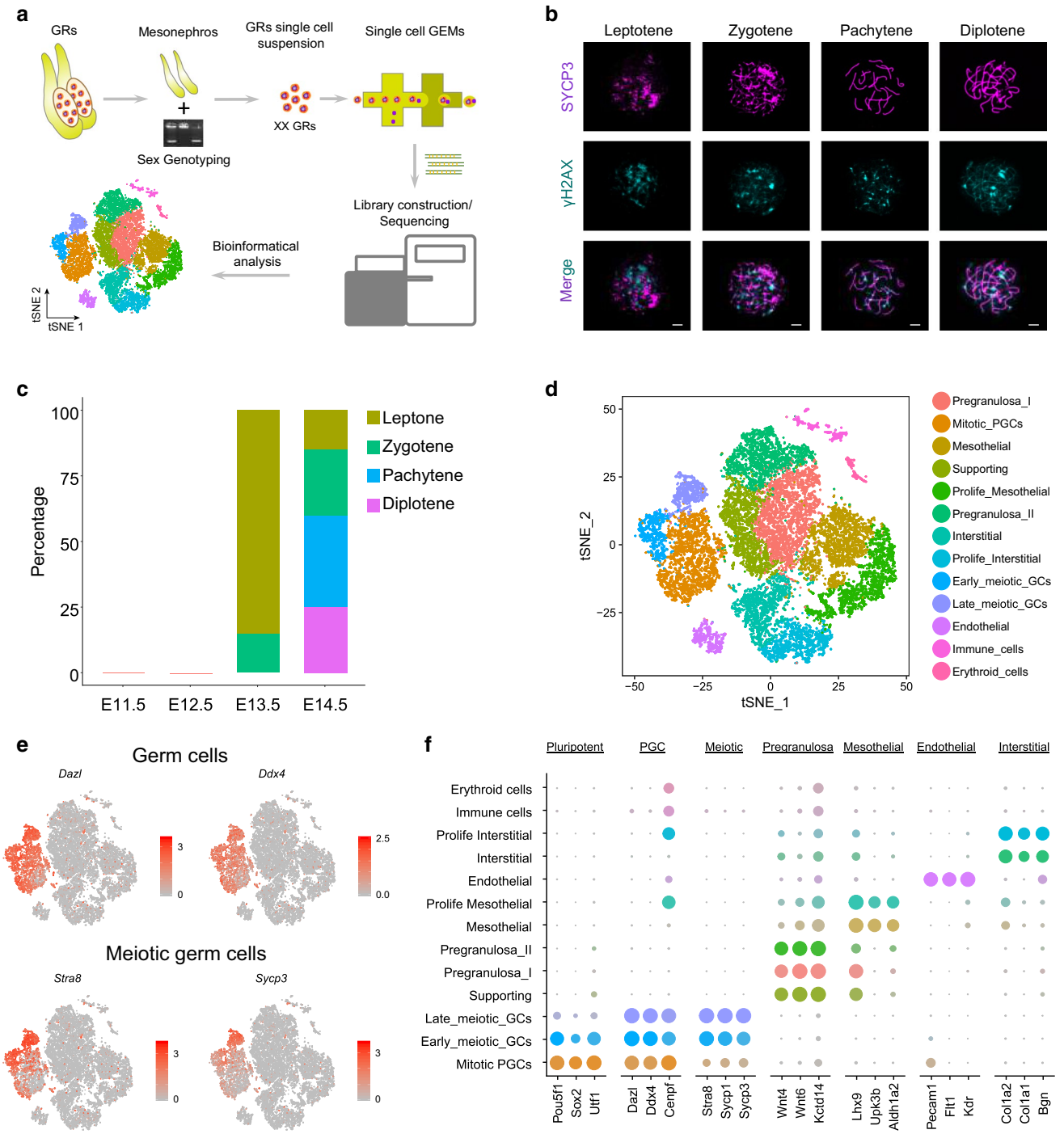

Fig. 1 Experimental design and characterization of single cell clusters. **a** Diagram of sample preparation for scRNA seq. **b** Representative SYCP3 and γH2AX staining of chromosome spreads at different meiotic progression stages (leptotene, zygotene, pachytene and diplotene) during meiosis prophase I. Scale bars 7.5 μm. **c** The percentage of premeiotic, leptotene, zygotene, pachytene, and diplotene stage germ cells at different developmental time-point (E11.5, E12.5, E13.5, E14.5). SYCP3 positive oocytes emerged at E13.5 with ~ 85% oocytes at the leptotene stage and ~ 15% oocytes at the zygotene stage in C57BL/6 mice. When the foetus reached E14.5 oocytes at the pachytene and diplotene stages were first detected (accounting for ~ 60% of total meiotic oocytes). **d** tSNE plot labelled with cell identities. tSNE analysis identified 13 cell clusters in the developing gonads, and each cell type was labelled with a different color. **e** Marker gene expression projected onto the tSNE plot. The marker genes used were: *Dazl*, *Ddx4* for germ cells; *Stra8*, *Sycp3* for meiotic germ cells. **f** Dot plot of the pluripotent, meiotic germ cell, pregranulosa cell, mesothelial cell, endothelial cell and interstitial cell marker expression across all cell types. Each cell cluster was color-coded with their identity. The dot size represents the percentage of cells expressed the indicated genes in each cluster and the dot color intensity represents the average expression level of the indicated genes

the GO terms of "meiotic cell cycle", "male meiotic nuclear division" and "cellular response to DNA damage stimulus", further confirming their entering into meiosis at these stages (Supplementary Fig. 2e). Among the somatic cells, granulosa cell lineage mainly enriched GO terms of "aldehyde biosynthetic process", "reproductive structure development" and "cellular response to extracellular stimulus" (Supplementary Fig. 2f). Meanwhile, the interstitial and mesothelial populations were both similarly enriched in the cell cycle-related GO terms, such as "regulation of mitotic cell cycle" and "mitotic cell cycle" (Supplementary Fig. 2g, h). Besides, interstitial cells enriched genes were involved in "blood vessel development" and mesothelial cells enriched genes were involved in "respiratory system development". Regarding endothelial cells, our analysis revealed that GO terms of "angiogenesis", "endothelial cell migration" and "endothelial cell proliferation" were enriched, further confirming their endothelial identity (Supplementary Fig. 2i).

High-resolution dissection of germ cell meiotic progression at single-cell resolution

To dissect germ cell meiotic progress at a higher resolution, we subclustered the three germ cell clusters and re-performed tSNE projection (Fig. 2a, b). Noteworthy, cell clustering using principal component analysis (PCA) algorithm distinguished three germ cell clusters, while tSNE algorithm identified seven distinct subclusters, further emphasizing the different cellular states during the progression of meiosis (Fig. 2a, right panel). More importantly, tSNE projection of all germ cells revealed seven transcriptionally distinct subclusters (Fig. 2b), and these identified clusters were more distinguishable when compared with PCA algorithm (Supplementary Fig. 3a). Similar to the results reported in Fig. 1d, we could also allocate the germ cells from E11.5 and E12.5 gonads mainly at the top of the tSNE plot and those from E13.5 and E14.5 at the middle and bottom of the tSNE plot, deciphering their entering and progression into meiosis (Fig. 2b, left panel). Interestingly, by analysing the top five cluster-specific expressed genes, we found that cluster 0 and 1 showed similar gene expression pattern, characterized by high expression of early meiotic markers *Stra8*, *Smc1b* and *Rec8*, while cluster 2, 3, 4 and 5 showed similar gene expression pattern, with high expression of *Dusp9*, *Wdr89,* and *Dppa5a* (Supplementary Fig. 3b). For cluster 6, they showed high levels of late meiotic markers *Sycp3*, *Tex101* and *Taf7l*. Taken together, the preliminary analysis demonstrated that the different germ cell clusters may represent different germ cell stages en route to meiosis.

We next visualized a series of typical marker genes of germ cells to assign them within each cluster: *Dppa5a*, *Utf1*, *Pou5f1* and *Sox2* for mitotic (premeiotic) PGCs, *Stra8*, *Rec8*, *Dazl* and *Smc1b* for early meiotic germ cells, and *Dmrtc2*, *Tex12*, *Tex15* and *Taf7l* for the late meiotic germ cells (Supplementary Fig. 3c) [5]. We found that mitotic PGCs were mainly allocated in subclusters 2, 4 and 5, while early meiotic markers mainly expressed in clusters 0, 1 and 3, and late meiotic markers showed the highest expression in cluster 6. Combined with the developmental point for each cell cluster (Fig. 2b, left panel), it is plausible that cluster 3 marks the primary population of germ cells which have initiated meiosis, while cluster 6 marks the late stage of germ cells during meiosis prophase I. Since we have successfully identified four transcriptional distinct populations (clusters 3, 1, 0 and 6) that marks the different stage of meiosis prophase I, we then proceed to investigate the sequential changes of all DEGs that drive the progression of meiosis by analysing the gene expression differences between different clusters. By analysing the DEGs expressions among mitotic clusters (mitotic 0, cluster 2, 4, 5), meiotic I (cluster 3), meiotic II (cluster 1). Meiotic III (cluster 0), and meiotic IV (cluster 6) that marks the progression of meiosis (Fig. 2c), we found that the earliest meiotic I stage significantly elevated classical meiosis "gatekeeper" genes *Stra8*, *Dazl*, *Dusp9* and *Smc1b* (encoding DNA recombination proteins) [5], while in the meiotic II stage, the expression of *Stra8*, *Smc1b,* and *Serf1* (encoding a protein with unknown function) was further elevated. Besides, synaptonemal complex protein family *Sycp1/3*, *Rec8* (a meiosis-specific component of the cohesins) [52] and *Taf7l* (well known for its role in regulating spermiogenesis) [53] were upregulated at this stage. For the latter two stages, *Sycp3*, *Taf7l*, *Tex15* (reported to be expressed in male meiotic germ cells) [54, 55] and *Dmrtc2* (doublesex and mab-3 related transcription factor-like family C2) [5] were continuously up-regulated. Noteworthy, *Prdm9* (a major determinant of meiotic recombination hotspots) [56] was significantly up-regulated in the late stage of meiosis, while *Pou5f1* and *Rec8* significantly decreased at this stage. Intriguingly, *Stk31*, a male germ cell-specific factor which was dispensable for spermatogenesis [57], was also detected during female meiosis prophase I (Fig. 2c), and our western blot analysis also confirmed its expression during female meiosis progression (Supplementary Fig. 3d), thus deciphering potential roles during female meiosis prophase I.

Besides, we further characterized the germ cell stage-specific marker gene expression (Fig. 2d). Similar to our analysis illustrated above, germ cells at meiotic I showed similar gene expression to mitotic stage germ cells except for high expression of *Dazl* and *Serf1*. As for germ cells at meiotic II and III, we observed elevated expression of meiosis markers such as *Stra8*, *Rec8* and *Tex12*, and decreased expression of mitotic cluster genes. For the meiotic IV stage germ cells, they specifically increased *Prdm9*, *Inca1*, *Sycp2*, *Syce3*, *Dmrtc2* and significantly decreased mitotic and meiotic I, II, III stage marker genes. We also compared the cluster enriched GO terms and the Circos plot demonstrated that

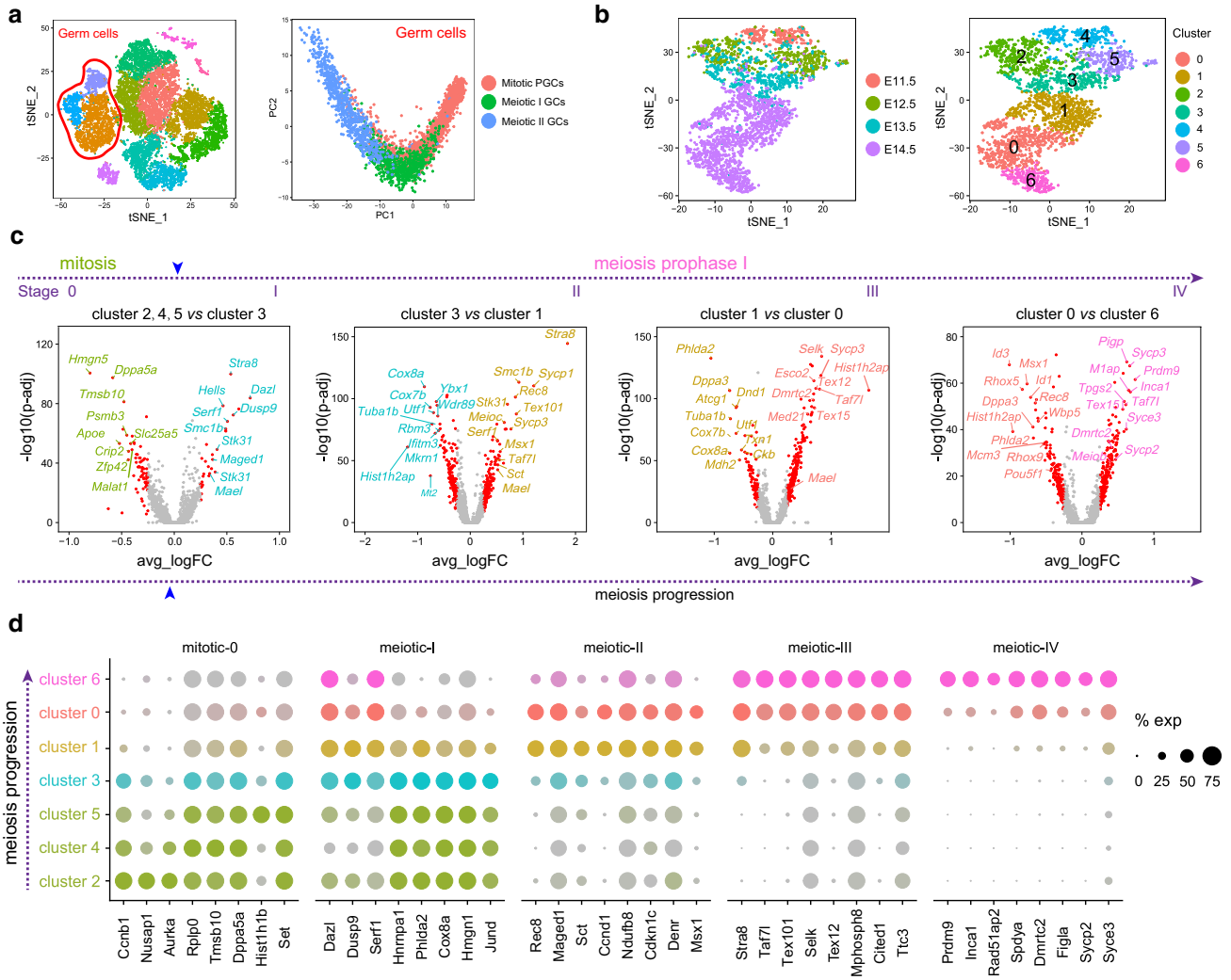

Fig. 2 Dissecting germ cell heterogeneity at a single-cell resolution. **a** Subclustering germ cell populations from the tSNE projection of all cells from the gonads. All germ cells were subclustered using Seurat (left) and were then analysed with PCA (right, colour-coded with the cell identity). **b** tSNE projection of all germ cells. Cells from E11.5, E12.5 and E13.5 showed a closely clustering pattern while E14.5 showed a discrete clustering pattern (left). Reforming tSNE analysis illustrated seven transcriptionally different sub-clusters (right). **c** Volcano plot demonstrating DEGs in different germ cell stages. Representative DEGs for each cluster were colour coded with corresponding cluster colours. Red dots represent significant DEGs while the grey dots represent non-significant DEGs. **d** Dot plot illustrating cluster-specific gene expression across all germ cell clusters. The dot size represents the percentage of cells expressing the indicated genes in each cluster and the dot colour intensity represents the average expression level of the indicated genes

clusters 0 (meiotic III) and 6 (meiotic IV) enriched many overlapped GO terms, including "synaptonemal complex assembly" and "meiotic cell cycle" (Supplementary Fig. 3e, f). As for clusters 2, 4 and 5, they similarly enriched GO terms of "mitotic cell cycle process" and "mitotic nuclear division" (Supplementary Fig. 3f), further confirming their mitotic germ cell identity.

Recapitulating gene regulatory networks (GRNs) underlying germ cell meiosis initiation

To recapitulate the gene regulatory relationships among the different germ cell clusters and infer the regulatory mechanisms underlying the germ cell status transition, we then used SCENIC, an algorithm developed to deduce GRNs and cellular status for scRNA data [31]. We, therefore, extracted the germ cell expression matrix from Seurat and imported them as the input matrix for SCENIC. By recognizing the co-expression modules (including transcriptional factors) and *cis*-regulatory motif analysis with each co-expression

modules, we obtained a series of cell identity-specific regulons together with their corresponding targets (Supplementary Table 2). Next, we used the AUCell algorithm to score the activity of each regulon in each cell according to the standard SCENIC pipeline and obtained the binary activity regulon matrix. To confirm our Seurat tSNE analysis based on the highly variable genes, we then reperformed cell clustering of germ cells based on the AUCell scored regulon activity as regulon activity was also cell identity specific as previously described [31]. Consistent with the Seurat tSNE algorithm, cell clustering using regulon activity also obviously distinguished mitotic, meiotic I, II, III and IV stage

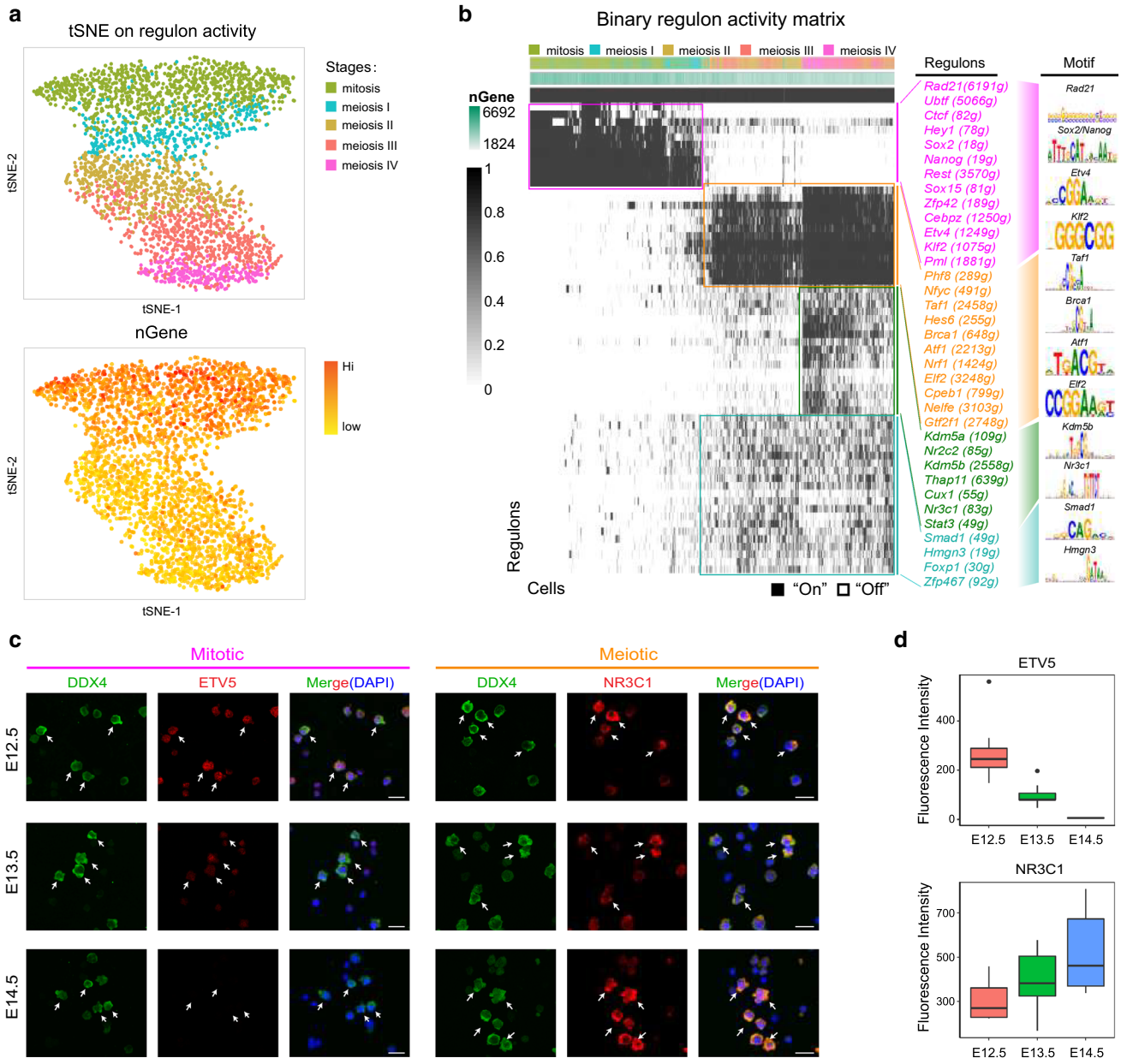

Fig. 3 Single-cell regulatory network inference and clustering in the germ cell clusters. **a** tSNE projection of all germ cells based on the binary regulon activity. Top: Cells are labelled with their Seurat-determined identity. Bottom: Gene density projected into the tSNE plot. The colour density represents the number of genes. **b** SCENIC binary regulon activity matrix showing the cell type-specific enrichment of regulons. Each column represents one single cell and each row represents one regulon. "On" represents active regulons and "Off" represents inactive regulons. **c** Immunofluorescence analysis of mitotic regulon ETV5 and meiotic regulon NR3C1 in E12.5, E13.5 and E14.5 ovarian cells; germ cells were stained with DDX4 and white arrows indicate ETV5/NR3C1 and DDX4 double-positive germ cells. Scale bars 25 μm. **d** Fluorescence intensity analysis of ETV5 and NR3C1 expression at E12.5, E13.5 and E14.5. The box represents the first quartile to the third quartile, while the thick line represents the median

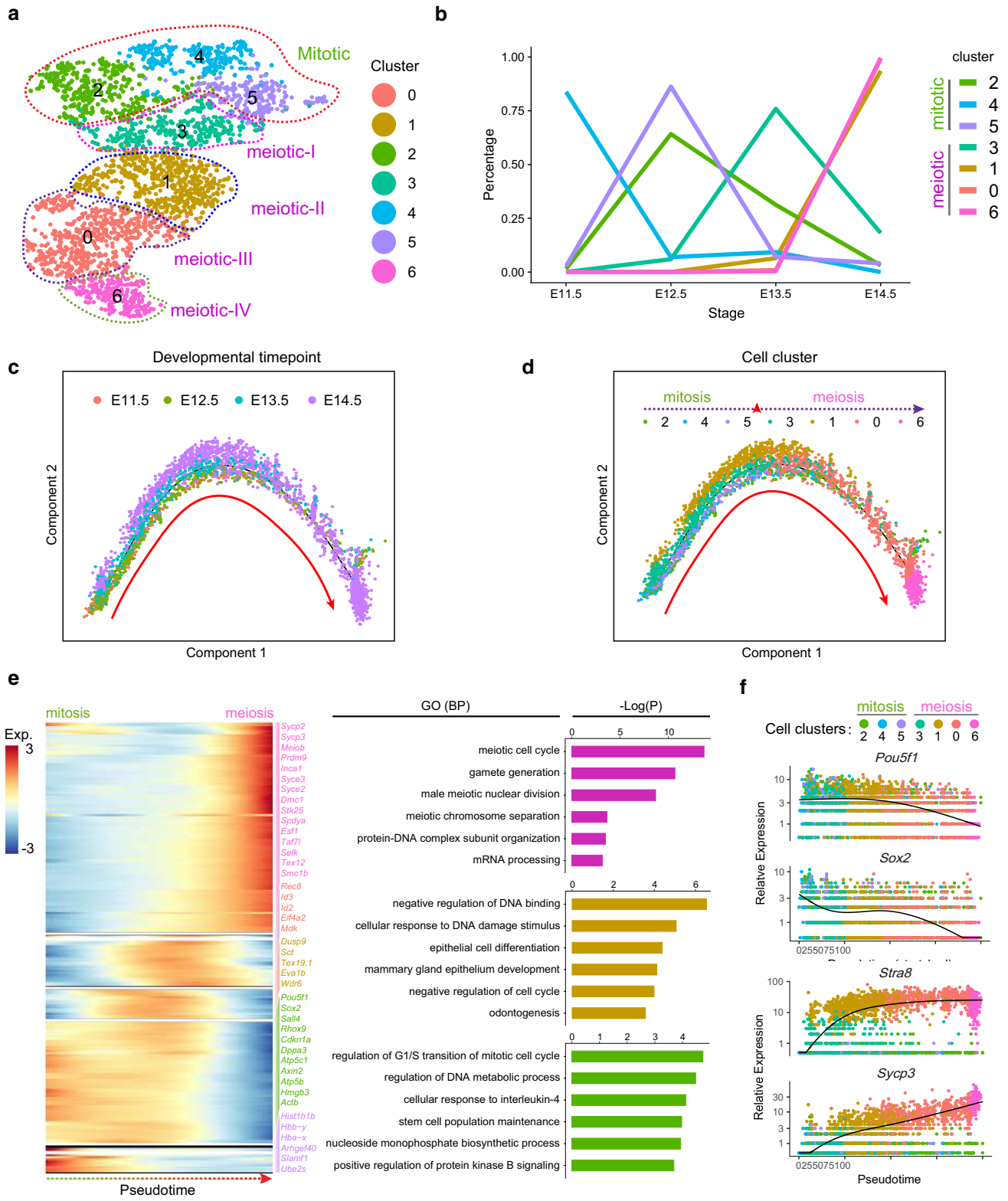

germ cells (Fig. 3a), confirming the *bona fide* characterization of cell identify by using aforementioned tSNE analysis.

Next, to recognize the master regulators within each cell population, we visualized regulon activity across all the germ cells based on the regulon scores calculated by AUCell. Noteworthy, the binary regulon activity heatmap indicated that mitotic germ cell clusters and meiotic I germ cell clusters predominantly showed high expression of

◂**Fig. 4** Pseudo-time ordering of all germ cells along meiosis progression. **a** tSNE projection of all germ cell clusters. Germ cells were divided into mitotic, meiotic I, meiotic II, meiotic III, meiotic IV germ cell clusters. **b** Line chart demonstrating the percentage of cells from different timepoint in each germ cell clusters. Clusters were colour-labelled corresponding to the tSNE plot. **c** Pseudo-time ordering of all germ cells coloured by their cell identity. Each dot was coloured according to their developmental time point. **d** Pseudo-time ordering of all germ cells coloured by their cell clusters. **e** Heatmap representing gene expression dynamics during pseudo-time ordering of all germ cells and GO enrichment analysis of DEGs from different gene sets. **f** Pseudo-time expression pattern of representative genes. Cells were coloured with their cluster information

regulons including *Sox2*, *Etv4* and *Nanog* regulons (Fig. 3b and Supplementary Fig. 4), all of which were well-defined regulators in the maintenance of pluripotency and self-renewal capacity of embryonic stem (ES) cells [58]. We also found that mitotic germ cells also enriched cell cycle-related regulon *Rad21and Rest* [59, 60], which was consistent with their mitotic cellular status. Interestingly, some of these regulons gradually "turned off" in the meiotic I germ cells clusters; it is, therefore, plausible that the down-regulation of mitotic specific expressed regulons (pluripotency and cell cycle-related) is pivotal for germ cells to initiate meiosis fate. Consistent with our analysis here, Yamaguchi et al. demonstrated that the NANOG protein was expressed in E11.5 and E12.5 germ cells while it was undetectable in E13.5 and E14.5 germ cells [61], which also confirmed our analysis here. Besides, immunofluorescence analysis of ETV5 showed that ETV5 mainly expressed at E12.5, E13.5 (Fig. 3c), while it was undetectable at E14.5 as revealed by fluorescence intensity analysis, further confirming our regulon analysis here (Fig. 3d).

For meiotic germ cell clusters (meiotic II, III and IV stage), they similarly enriched a series of regulons, including *Phf8* (encoding a histone lysine demethylase) [62], *Taf1* (interact directly with TATA-binding protein) [63], *Brca1* (highly expressed in pachytene and diplotene spermatocytes) [64], *Elf2* (a rhombotin-2 binding ets transcription factor) [65], etc. Noteworthy, a series regulon was gradually "turned on" meiotic IV stage germ cells, including *Kdm5a* (encoding a histone demethylase) [66], *Nr3c1* (encoding a glucocorticoid receptor with transcription or co-transcription factor functions) [67] and *Stat3* (critical for meiotic cell cycle) [68]. Immunofluorescence of the meiotic regulon NR3C1 showed that NR3C1 was specifically expressed in germ cells and that its expression increased with the progression of meiosis, thus deciphering potential roles during the progression of meiosis (Fig. 3c, d).

Pseudo-time reconstruction of meiosis progression trajectory

According to the tSNE projection, we successfully identified mitotic PGCs, meiotic I, II, III and IV stage germ cells and delineated their detailed signature gene expression patterns during germ cell meiosis initiation (Fig. 4a). Interestingly, the percentage of meiotic I stage germ cells significantly increased at E13.5, while the percentage of meiotic II, III and IV significantly increased at E14.5 (Fig. 4b). To reconstruct the pseudo-time trajectory of germ cells during meiotic progression, we used variable genes identified by Seurat as ordering genes (Supplementary Fig. 5a) and performed pseudo-time ordering of all germ cells using Monocle, a new and improved algorithm for classifying and counting cells, performing differential expression analysis between the subpopulations of cells [69]. After construction of the germ cell lineage trajectory, we observed an inverted "U" structure with cells from E11.5 and E14.5 distributed at the two terminals (Fig. 4c), which was also consistent with their relationship from the perspective of developmental timepoint. Besides, we also analysed cell cluster distribution along pseudo-time, and it was found that the precedence relationship identified according to their gene expression pattern was also consistent with Monocle analysis here, with mitosis cell populations (cluster 2, 4, 5) distributed at the left and meiotic cell clusters (cluster 3, 1, 0, 6) distributed at the right (Fig. 4d), further demonstrating the progression of meiosis.

To gain in-depth insight into the gene expression dynamics during the initiation of meiosis, we analysed gene expression dynamics along pseudo-time and observed five distinct DEG (q val $< 1e{-}4$) sets according to k-means clustering (Fig. 4e). We also performed GO enrichment to investigate the gene function categories of these DEGs and it was found that at the early stage (gene set 2), germ cells significantly expressed genes enriched in GO terms of "regulation of G1/S transition of mitotic cell cycle" and "regulation of DNA metabolic process", while in the middle stage (gene set 3), germ cells expressed genes mainly enriched in GO terms of "negative regulation of DNA binding" and "cellular response to DNA damage stimulus". At the endpoint of pseudo-time trajectory, germ cells expressed genes enriched in GO terms of "meiotic cell cycle" and "gamete generation". Besides, we also evaluated pluripotent marker *Pou5f1*, *Sox2, Sall4, Dppa3, Eif4a1 and Rhox9* [70] expression levels along pseudo-time and found that *Pou5f1*, *Dppa3*, *Eif4a1* and *Rhox9* significantly decreased when germ cells initiated meiotic program while the expression of *Sox2* and *Sall4* continuously decreased along pseudo-time (Fig. 4f and Supplementary Fig. 5b). For meiotic markers, *Stra8*, *Sycp3*, *Prdm9*, *Sycp2*, *Taf7l* and *Tex12*, they all showed elevated levels along pseudo-time, which was also consistent with

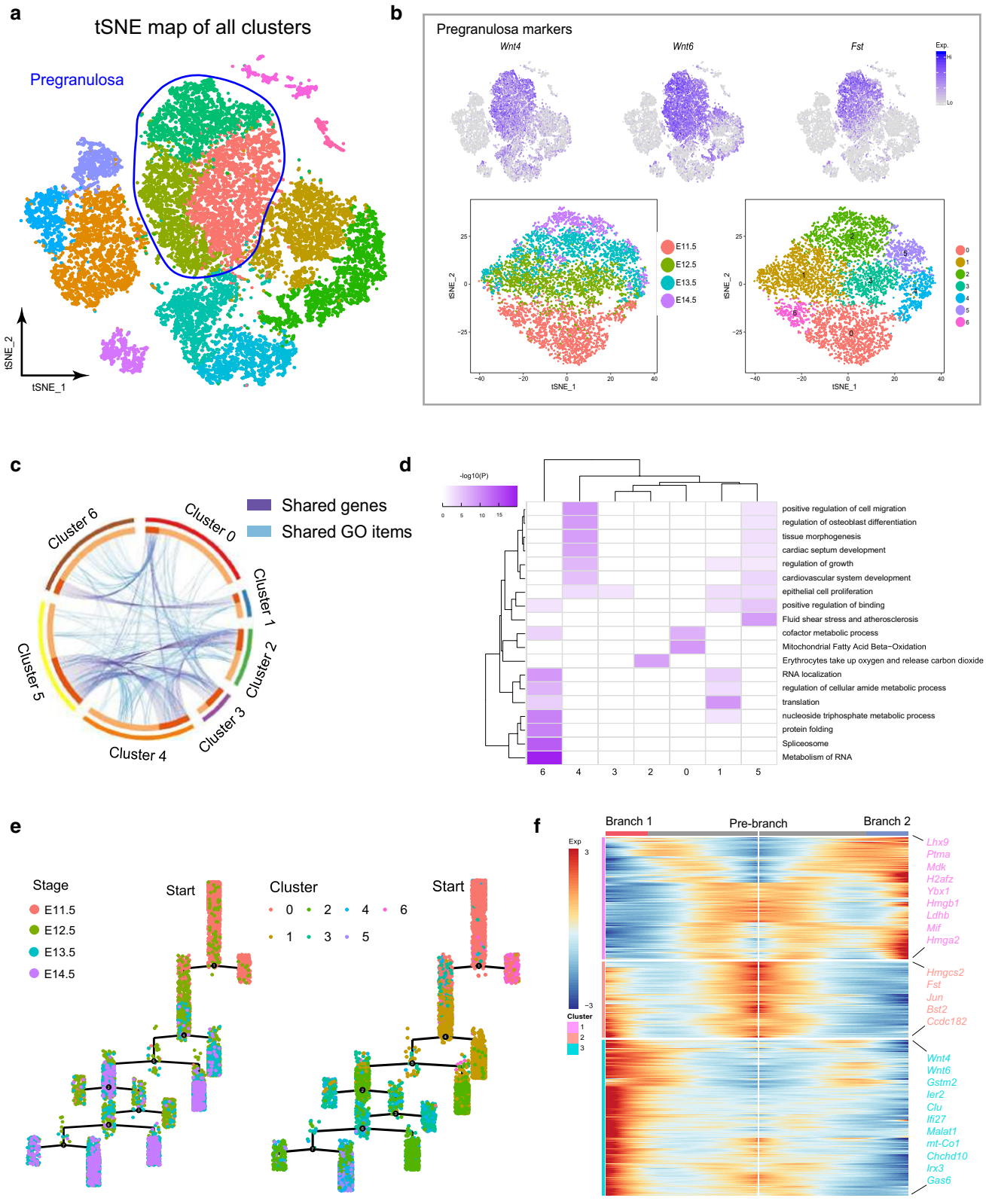

our previous DEGs analysis. Noteworthy, the expression of *Prdm9* and *Sycp2* was elevated in the late stage of meiosis, thus emphasizing their roles in the late stage of meiotic progression. Taken together, our data here characterized

◂**Fig. 5** Dissecting granulosa lineage cellular heterogeneity along the progression of meiosis. **a** Pregranulosa cell population highlighted in the tSNE plot. **b** Top: Identification of pregranulosa cell markers *Wnt4*, *Wnt6* and *Fst* expression in the tSNE plot of all cell clusters. Bottom: tSNE projection of pregranulosa cell clusters. Cells are labelled with sample ID and cluster ID, respectively, and tSNE analysis reveals 6 subclusters in pregranulosa lineage cells. **c** Circos plot displaying shared DEGs and shared GO terms between different pregranulosa cell clusters. Shared DEGs were labelled with purple lines and shared GO terms were labelled with light blue lines. **d** Heatmap demonstrating the enrichment of GO terms in each pregranulosa cell cluster. Each row represents GO terms and each column represents cell clusters. **e** Pseudo-time ordering of all pregranulosa cells by Monocle. The distance from a cell to the root corresponds to pseudo-time. **f** Heatmap representing gene expression dynamics during pseudo-time ordering of pregranulosa cells. The branch point represents branch point 4 in Fig. 5e

detailed germ cell gene expression dynamics along meiosis progression and provided us an in-depth insight into the molecular mechanisms underlying meiosis regulation.

Dissecting heterogeneity and cellular fate decisions of the granulosa cell lineage

After the initial identification of the supporting and pregranulosa cell clusters, we then re-performed tSNE analysis on *Wnt4*, *Wnt6* and *Fst* positive cell populations to preliminarily investigate the cellular heterogeneity of the identified supporting cell and pregranulosa cell clusters, as granulosa cells have been demonstrated to interact with an oocyte to promote oocyte development (Fig. 5a, b) [71]. tSNE projection resulted in seven subclusters showing distinct developmental-dependent dynamics (Fig. 5b lower panel and Supplementary Fig. 6a), each characterized by a specific gene profile (Supplementary Fig. 6b).

The comparison of the shared DEGs and GO terms showed that subcluster 0 shared the GO terms of "cofactor metabolic process" with subcluster 6, while subclusters 2, 3, 4 and 5 shared more GO terms (Fig. 5c, d). Combined with their cell label information, we found that subclusters 0, 1 and 6 were mainly composed of cells from E11.5 and E12.5, while subclusters 2, 3 and 5 were mainly composed of cells from E13.5 and E14.5 (Fig. 5b), which likely delineates the differentiation of supporting cells into pregranulosa cells. We then reconstructed the pseudo-time ordering of all granulosa cell lineage precursors and it was revealed that within the four developmental points, granulosa cell lineage precursors branched into multiple developmental branches (Fig. 5e and Supplementary Fig. 6c). This suggested a high heterogeneity of granulosa cell lineage precursors during meiotic initiation. To define more precisely the gene expression transition during the cell fate decision from supporting cells into pregranulosa cells, between E12.5 and E13.5, we performed DEG comparisons on the pseudo-time ordering of these cells (Fig. 5f). We observed three sets of DEGs and for the pre-branch lineage, DEGs enriched the GO terms of "organic acid catabolic process and small molecular biosynthetic process", while branch 1 (characterized by elevated expression of *Wnt4* and *Wnt6*) and branch 2 (characterized by expression of *Lhx9* and *Ptma*) enriched the GO terms of "actin filament-based process, positive regulation of cell death" and "ribonucleoprotein complex biogenesis, translation", respectively (Supplementary Fig. 6d, e).

Mesothelial and interstitial cell populations show two distinct cellular states

In our aforementioned tSNE projection of somatic cell clusters, it was observed that two mesothelial, two interstitial and one endothelial cell population(s) can be characterized (Fig. 6a). Interestingly, the preliminary analysis indicated that the clusters within the interstitial and mesothelial cells expressed a similar level of *Bgn* and *Upk3b*, which we had used to mark interstitial and mesothelial, respectively (Fig. 6b, top panel). However, the expression of cell cycle-related genes, such as *Cdk1*, *Ccna2* and *Cenpa*, showed specific expression only in interstitial cluster 2 and mesothelial cluster 4 (Fig. 6b, lower panel). To gain further insight into the transcriptome differences between the cell clusters, we then compared the top100 expressed DEGs between the four clusters. The Venn diagram demonstrated that cluster 2 from interstitial cells and cluster 4 from mesothelial shared a very high percentage of overlapped DEGs (Fig. 6c, left). Besides, protein to protein interaction network analysis suggested that the 41 co-expressed DEGs mainly enriched in "cell cycle-related network" (Fig. 6c, right panel). GO analysis also indicated that the co-expressed DEGs enriched the GO terms of "cell division", "regulation of mitotic cell cycle" and "mitotic prophase" (Fig. 6d), suggesting that clusters 2 and 4 shared a similar cellular status. As for cluster 1 and cluster 3, GO enrichment analysis showed that cluster 1 enriched the GO terms of "cardiovascular system development", "circulatory system development" and "tissue development" and cluster 3 enriched the GO terms of "organ development", "system development", and "anatomical structure development" (Supplementary Table 3). On the whole, these results suggest that during the early stages of ovary development interstitial and mesothelial cells possess two cellular states, one primed to differentiation and another to self-renew.

Finally, we analysed the interstitial, mesothelial and endothelial cells at a higher resolution by extracting the three cell populations and re-performing tSNE visualization analysis. The tSNE projection revealed three subclusters for endothelial cells and five subclusters each for interstitial and mesothelial cells (Supplementary Fig. 7a). We next compared the top five DEGs among the clusters and found that cluster 1, 2 in interstitial, cluster 2, 3, 4 in mesothelial

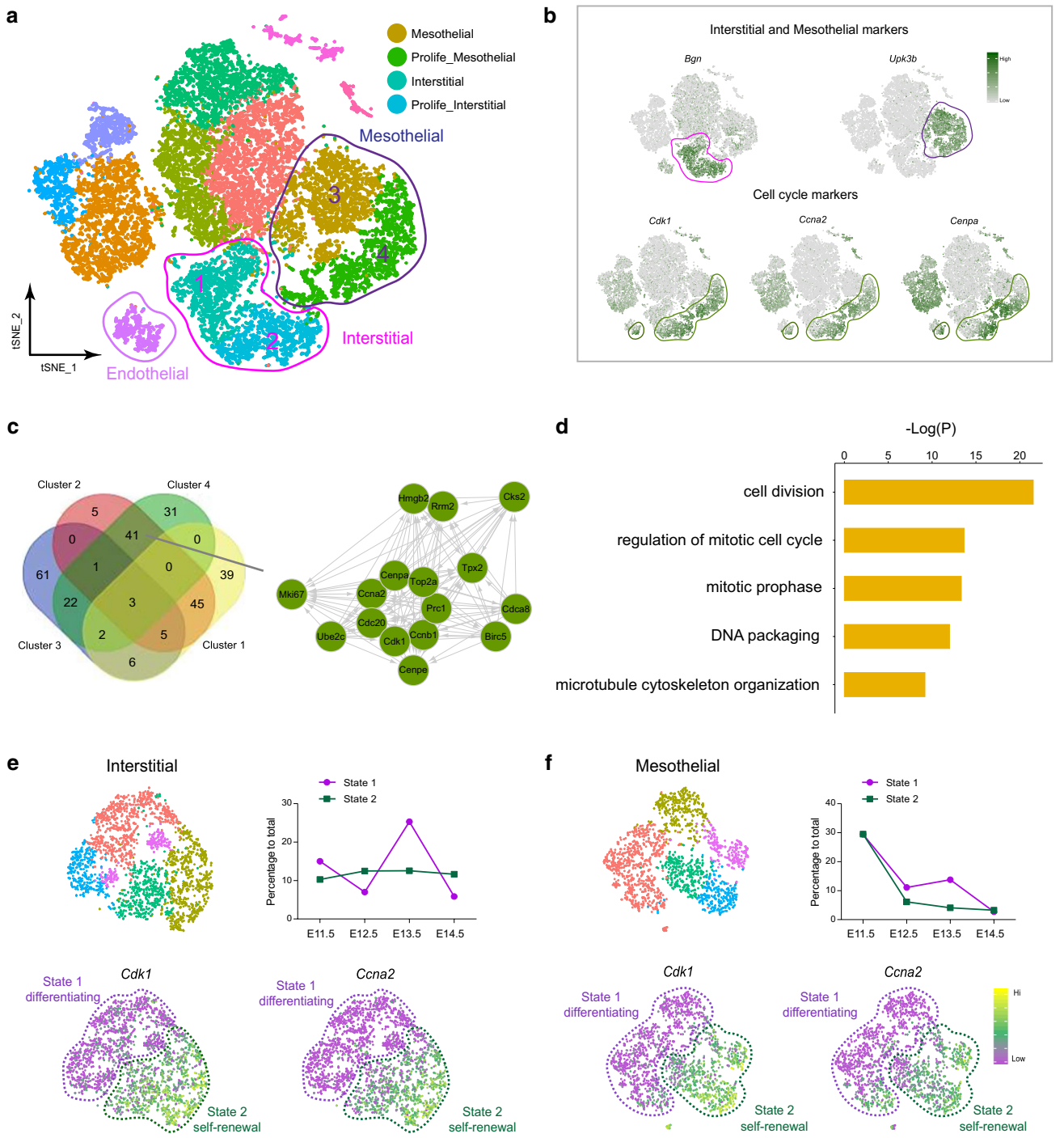

Fig. 6 Dissecting interstitial and mesothelial heterogeneity by using scRNA seq. **a** Interstitial and mesothelial cell populations are highlighted in the tSNE plot. **b** Visualizing the expression of the interstitial marker (*Bgn*), mesothelial marker (*Upk3b*) and the cell cycle-related genes (*Cdk1*, *Ccna2* and *Cenpa*) in the tSNE plot. **c** Venn plot demonstrating the overlap of co-expressed DEGs between the interstitial and mesothelial subclusters. Cluster 2 and cluster 4 co-expressed DEGs were extracted to perform protein–protein network analysis using STRING database. **d** Top enriched GO terms of co-expressed DEGs between cluster 2 and cluster 4. **e** Reperforming tSNE analysis on interstitial clusters and visualization of cell status dynamics and cell cycle-related marker genes (*Cdk1* and *Ccna2*). Interstitial clusters were extracted to reperform tSNE analysis. We termed subclusters expressing a high level of cell cycle-related genes as "State 2" and the remaining "State 1". **f** Reperforming tSNE analysis on mesothelial clusters and visualization of cell status dynamics and cell cycle-related markers genes (*Cdk1* and *Ccna2*). Mesothelial clusters were extracted to reperform tSNE analysis. We termed subclusters expressing a high level of cell cycle-related genes as "State 2" and the remaining "State 1"

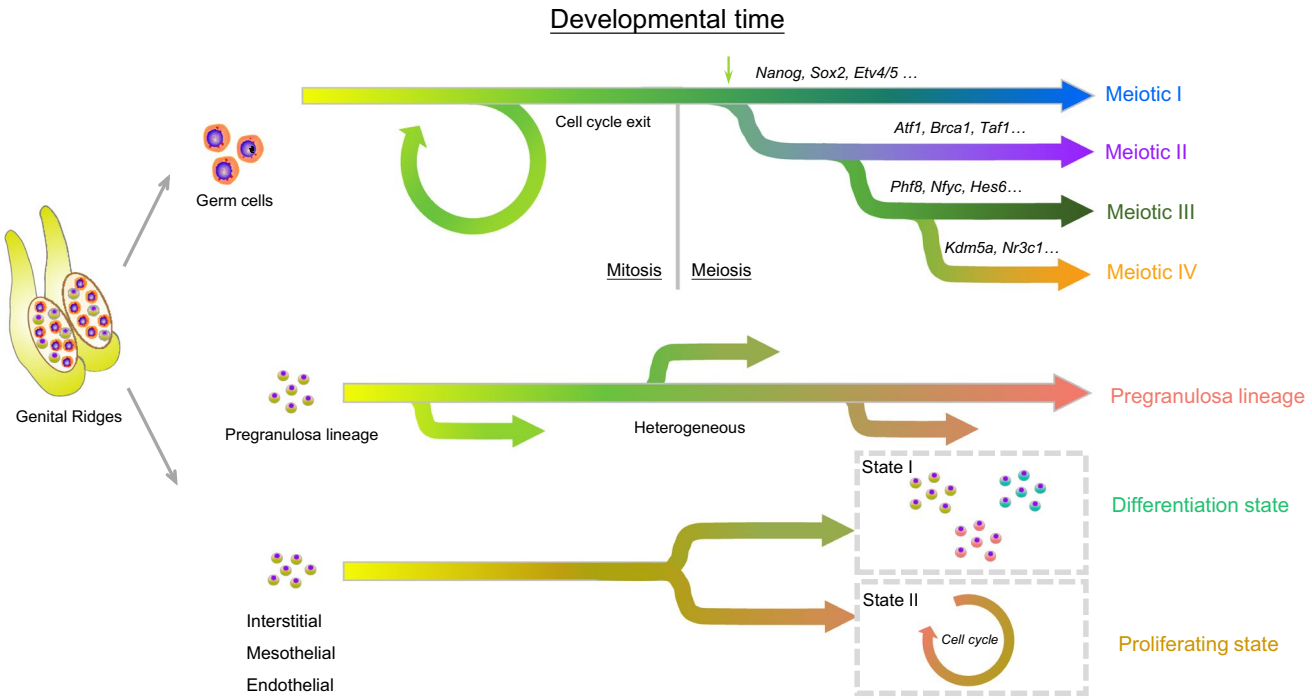

Fig. 7 Model of the cellular dynamics in female gonads during the initiation of meiosis in germ cells. Germ cells are highly proliferative with a linage priority to meiosis initiation and express high levels of cell cycle-related genes at E11.5 and E12.5. At around E13.5, a small population of germ cells initiate meiosis and this process is asynchronous in mice. Granulosa cell lineage cells are highly heterogeneous during this stage and the interstitial, mesothelial and endothelial cells reveal two cellular states: one showing "differentiating" characteristics, while the other displays "self-renewing" characteristics

cells and a portion of cluster 1, 2 in endothelial cells showed higher expression of cell cycle-related genes, such as *Top2a*, *Cenpa* and *Cdk1* (Supplementary Fig. 7b, c). This illustrated that interstitial, mesothelial and also endothelial populations possess two cellular states. Furthermore, it was found that the percentage of interstitial cells with "differentiating" status was higher at E13.5 while the "self-renewal" state remained quite constant (Fig. 6e). On the other hand, in the mesothelial cells the percentage of both states progressively decreased alongside developmental time (Fig. 6f).

Discussion

The scRNA-seq technology facilitates the identification of new cell types and gene regulatory networks as well as allowing dissection of the kinetics and patterns of allele-specific gene expression [72, 73]. In such studies, individual cells are executing gene expression programs in an unsynchronized manner. Single-cell gene expression studies enable profiling of transcriptional regulation during complex biological processes and within highly heterogeneous cell populations. These studies allow the discovery of genes that identify certain subtypes of cells, or that mark an intermediate status during a biological process [74].

In the present paper, we used such an approach, for the first time, provided new insights into molecular events underlying meiosis initiation and progression into prophase I in female mouse germ cells. We used an experimental model to characterize gene expression profiles of the heterogonous somatic cell populations present within the sex differentiating ovaries. To validate such analyses and separate biological variability from the possible technical noise that might affect scRNA-seq protocols, we employed various algorithms and bioinformatics analyses, the soundness of our analyses was confirmed. By utilizing scRNA-seq on the fetal ovary during the periods of PGC proliferation (E11.5–E13.5), initiation and progression of meiosis (E13.5–E14.5), we successfully characterized molecular landscape during mitosis–meiosis transition based on the expression of marker genes in PGCs before (*Pou5f1*, *Sox2* and S*all4*), and at meiotic initiation (*Dazl*, *Stra8, Smc1b* and *Rec8*), and later oocytes (*Dmrtc2, Tex12, Tex15* and *Taf7l*).

The tSNE algorithm projection of the transcriptome data allowed clustering of four distinct populations of premeiotic PGCs and four germ cell populations in meiotic prophase I and their dynamics throughout the developmental period studied [28]. Several new genes highly expressed by each of these populations were also found. In total, 634, 654 and 1189 DEGs were identified in premeiotic, early and late

meiotic germ cells, respectively. By focusing on the germ cell populations using tSNE, we observed seven germ cell clusters along meiosis progression. Noteworthy, we characterized four transcriptionally distinct meiotic germ cell clusters during meiosis prophase I. By analysing their DEGs expression along meiosis progression, we delineated detailed gene expression landscape during meiosis progression in mice. For the meiotic initiation, our analysis demonstrated that *Stra8*, *Dazl*, *Dusp9*, *Hells* and *Serf1* were significantly up-regulated DEGs in meiotic I stage germ cells. For the late stage of meiosis, we observed DEGs such as *Pigp*, *Sycp3*, *Prdm9*, *Taf7l* and *Syce3*. Noteworthy, except for the classical *Stra8*, *Dazl*, *Sycp3* and *Prdm9*, the roles of *Dusp9*, *Hells*, *Serf1*, *Pigp* and *Taf7l* in meiosis progression remain little known and future studies aimed to unravel the role that some of these genes play during meiosis should provide critical information about early gametogenesis in mammals. Noteworthy, by utilizing the same scRNA-seq technology, Li et al. characterized detailed transcriptome landscape during human germ cell development at various developmental stages and reported transcriptional profiles of the mitotic, RA responsive, meiotic, and oogenesis stage female germ cells [75]. Intriguingly, for mitotic germ cells, both human and murine germ cells showed high-level expression of pluripotent markers such as *Pou5f1* and *Nanog*, while *Stra8* was significantly elevated at the initiation stage of meiosis. At the meiosis stage, genes such as *Tex12*, *Tex14*, *Dazl*, *Mael,* and *Prdm9* showed elevated expression in both human and murine germ cells, further emphasizing the conserved roles of these genes during mammalian meiosis. Besides, it's also worth noting that our study further divided meiotic prophase germ cells into four sub-stages, which was not reported in human germ cells.

We also identified master regulons of germ cells which may drive the meiotic progression in mitotic, meiotic I, II, III and IV stage germ cells. For example, regulons such as *Etv4*, *Sox2* and *Nanog,* involved in the maintenance of pluripotency and self-renewal capacity of ES cells were predominantly expressed in mitotic PGCs, confirming their similarities with ES cells [76, 77]. While it could be expected that late meiotic germ cells, which involved extensive chromatin rearrangement, express the regulon *Hmgn3* encoding a nucleosome-binding protein thought to modulate the compactness of the chromatin fiber. The meaning of the expression of *Nr3c1*, encoding a glucocorticoid receptor with transcription or co-transcription factor functions, is intriguing but remains unexplained. Similarly, the implications of the prevalent expression in late meiotic germ cells of the regulons *Phf8*, a histone lysine demethylase, *Nfyc* a transcription encodes one subunit of a trimeric complex, *Kdm5a*, a histone demethylase and *Nelfe*, encoding a protein that represses RNA polymerase II transcript elongation, remain to be investigated. Collectively, these analyses here reveal the unique GRNs and master regulons in germ cells at different cellular stages during meiosis progression.

Our research also preliminarily investigated the transcriptome profiles of the four ovarian somatic cell lineages differentiating in the embryonic ovary during the initiation and progression of meiosis, namely pregranulosa, interstitial, mesothelial and endothelial cells. For pregranulosa cells, the package Monocle revealed multiple differencing branches supporting a high initial heterogeneity of cells in this lineage. In addition, interstitial cells and mesothelial cells showed two distinct cellular states that we defined as "self-renewing" and "differentiating" according to their transcriptome profiles.

In conclusion, the present data represent a new important resource for deciphering the molecular pathways driving meiosis initiation and progression in female germ cells and ovarian somatic cells (Fig. 7), thereby improving our understanding of the embryonic processes involved during gonadal development in female mammals. These results, prospectively, provide valuable information about the aetiology of human reproductive defects arising from dysregulation during early gametogenesis.

Acknowledgements We would like to thank all members of the Institute of Reproductive Sciences, Qingdao Agricultural University for their kind help during preparing single-cell samples and suggestions for preparing the manuscript. This work was supported by the National Key Research and Development Program of China (2018YFC1003400), National Nature Science Foundation (31671554 and 31970788) and Taishan Scholar Construction Foundation of Shandong Province (ts20190946).

Author contributions WG and WS: conceived and designed the experiments; WG, JW, RZ, ST, FZ, WL, LL, XS and SC: performed the experiments; WG, PD, MDF and WS: wrote and edited the manuscript.

Compliance with ethical standards

Conflict of interest The authors declare no conflict of interest.

References

1. Cinalli RM, Rangan P, Lehmann R (2008) Germ cells are forever. Cell 132(4):559–562. https://doi.org/10.1016/j.cell.2008.02.003
2. De Felici M (2016) The formation and migration of primordial germ cells in mouse and man. Results Probl Cell Differ 58:23–46. https://doi.org/10.1007/978-3-319-31973-5_2
3. Grive KJ, Freiman RN (2015) The developmental origins of the mammalian ovarian reserve. Development 142(15):2554–2563. https://doi.org/10.1242/dev.125211
4. Wang C, Zhou B, Xia G (2017) Erratum to: Mechanisms controlling germline cyst breakdown and primordial follicle formation. Cell Mol Life Sci CMLS 74(14):2567. https://doi.org/10.1007/s00018-017-2499-8

5. Handel MA, Schimenti JC (2010) Genetics of mammalian meiosis: regulation, dynamics and impact on fertility. Nat Rev Genet 11(2):124–136. https://doi.org/10.1038/nrg2723
6. Ge W, Chen C, De Felici M, Shen W (2015) In vitro differentiation of germ cells from stem cells: a comparison between primordial germ cells and in vitro derived primordial germ cell-like cells. Cell Death Dis 6:e1906. https://doi.org/10.1038/cddis.2015.265
7. Tucker EJ, Grover SR, Bachelot A, Touraine P, Sinclair AH (2016) Premature ovarian insufficiency: new perspectives on genetic cause and phenotypic spectrum. Endocr Rev 37(6):609–635. https://doi.org/10.1210/er.2016-1047
8. Saitou M, Miyauchi H (2016) Gametogenesis from pluripotent stem cells. Cell Stem Cell 18(6):721–735. https://doi.org/10.1016/j.stem.2016.05.001
9. Yamashiro C, Sasaki K, Yabuta Y, Kojima Y, Nakamura T, Okamoto I, Yokobayashi S, Murase Y, Ishikura Y, Shirane K, Sasaki H, Yamamoto T, Saitou M (2018) Generation of human oogonia from induced pluripotent stem cells in vitro. Science 362(6412):356–360. https://doi.org/10.1126/science.aat1674
10. Handel MA, Eppig JJ, Schimenti JC (2014) Applying "gold standards" to in vitro-derived germ cells. Cell 157(6):1257–1261. https://doi.org/10.1016/j.cell.2014.05.019
11. Sun YC, Cheng SF, Sun R, Zhao Y, Shen W (2014) Reconstitution of gametogenesis in vitro: meiosis is the biggest obstacle. J Genet Genom 41(3):87–95. https://doi.org/10.1016/j.jgg.2013.12.008
12. Tedesco M, Farini D, De Felici M (2011) Impaired meiotic competence in putative primordial germ cells produced from mouse embryonic stem cells. Int J Dev Biol 55(2):215–222. https://doi.org/10.1387/ijdb.103108mt
13. Hikabe O, Hamazaki N, Nagamatsu G, Obata Y, Hirao Y, Hamada N, Shimamoto S, Imamura T, Nakashima K, Saitou M, Hayashi K (2016) Reconstitution in vitro of the entire cycle of the mouse female germ line. Nature 539(7628):299–303. https://doi.org/10.1038/nature20104
14. Zhou Q, Wang M, Yuan Y, Wang X, Fu R, Wan H, Xie M, Liu M, Guo X, Zheng Y, Feng G, Shi Q, Zhao XY, Sha J, Zhou Q (2016) Complete meiosis from embryonic stem cell-derived germ cells in vitro. Cell Stem Cell 18(3):330–340. https://doi.org/10.1016/j.stem.2016.01.017
15. Griswold MD, Hogarth CA, Bowles J, Koopman P (2012) Initiating meiosis: the case for retinoic acid. Biol Reprod 86(2):35. https://doi.org/10.1095/biolreprod.111.096610
16. Bowles J, Knight D, Smith C, Wilhelm D, Richman J, Mamiya S, Yashiro K, Chawengsaksophak K, Wilson MJ, Rossant J, Hamada H, Koopman P (2006) Retinoid signaling determines germ cell fate in mice. Science 312(5773):596–600. https://doi.org/10.1126/science.1125691
17. Farini D, Scaldaferri ML, Iona S, La Sala G, De Felici M (2005) Growth factors sustain primordial germ cell survival, proliferation and entering into meiosis in the absence of somatic cells. Dev Biol 285(1):49–56. https://doi.org/10.1016/j.ydbio.2005.06.036
18. Miyauchi H, Ohta H, Nagaoka S, Nakaki F, Sasaki K, Hayashi K, Yabuta Y, Nakamura T, Yamamoto T, Saitou M (2017) Bone morphogenetic protein and retinoic acid synergistically specify female germ-cell fate in mice. EMBO J 36(21):3100–3119. https://doi.org/10.15252/embj.201796875
19. Small CL, Shima JE, Uzumcu M, Skinner MK, Griswold MD (2005) Profiling gene expression during the differentiation and development of the murine embryonic gonad. Biol Reprod 72(2):492–501. https://doi.org/10.1095/biolreprod.104.033696
20. Houmard B, Small C, Yang L, Naluai-Cecchini T, Cheng E, Hassold T, Griswold M (2009) Global gene expression in the human fetal testis and ovary. Biol Reprod 81(2):438–443. https://doi.org/10.1095/biolreprod.108.075747
21. Molyneaux KA, Wang Y, Schaible K, Wylie C (2004) Transcriptional profiling identifies genes differentially expressed during and after migration in murine primordial germ cells. Gene Expr Patterns: GEP 4(2):167–181. https://doi.org/10.1016/j.modgep.2003.09.002
22. Morohaku K, Hirao Y, Obata Y (2017) Development of fertile mouse oocytes from mitotic germ cells in vitro. Nat Protoc 12(9):1817–1829. https://doi.org/10.1038/nprot.2017.069
23. Chuma S, Nakatsuji N (2001) Autonomous transition into meiosis of mouse fetal germ cells in vitro and its inhibition by gp130-mediated signaling. Dev Biol 229(2):468–479. https://doi.org/10.1006/dbio.2000.9989
24. Li Y, Zheng M, Lau YF (2014) The sex-determining factors SRY and SOX9 regulate similar target genes and promote testis cord formation during testicular differentiation. Cell Rep 8(3):723–733. https://doi.org/10.1016/j.celrep.2014.06.055
25. Feng YM, Liang GJ, Pan B, Qin XS, Zhang XF, Chen CL, Li L, Cheng SF, De Felici M, Shen W (2014) Notch pathway regulates female germ cell meiosis progression and early oogenesis events in fetal mouse. Cell Cycle 13(5):782–791. https://doi.org/10.4161/cc.27708
26. Ge W, Ma HG, Cheng SF, Sun YC, Sun LL, Sun XF, Li L, Dyce P, Li J, Shi QH, Shen W (2015) Differentiation of early germ cells from human skin-derived stem cells without exogenous gene integration. Sci Rep 5:13822. https://doi.org/10.1038/srep13822
27. Ge W, Zhao Y, Lai FN, Liu JC, Sun YC, Wang JJ, Cheng SF, Zhang XF, Sun LL, Li L, Dyce PW, Shen W (2017) Cutaneous applied nano-ZnO reduce the ability of hair follicle stem cells to differentiate. Nanotoxicology 11(4):465–474. https://doi.org/10.1080/17435390.2017.1310947
28. Butler A, Hoffman P, Smibert P, Papalexi E, Satija R (2018) Integrating single-cell transcriptomic data across different conditions, technologies, and species. Nat Biotechnol 36(5):411–420. https://doi.org/10.1038/nbt.4096
29. Trapnell C, Cacchiarelli D, Grimsby J, Pokharel P, Li S, Morse M, Lennon NJ, Livak KJ, Mikkelsen TS, Rinn JL (2014) The dynamics and regulators of cell fate decisions are revealed by pseudotemporal ordering of single cells. Nat Biotechnol 32(4):381–386. https://doi.org/10.1038/nbt.2859
30. Qiu X, Hill A, Packer J, Lin D, Ma YA, Trapnell C (2017) Single-cell mRNA quantification and differential analysis with Census. Nat Methods 14(3):309–315. https://doi.org/10.1038/nmeth.4150
31. Aibar S, Gonzalez-Blas CB, Moerman T, Huynh-Thu VA, Imrichova H, Hulselmans G, Rambow F, Marine JC, Geurts P, Aerts J, van den Oord J, Atak ZK, Wouters J, Aerts S (2017) SCENIC: single-cell regulatory network inference and clustering. Nat Methods 14(11):1083–1086. https://doi.org/10.1038/nmeth.4463
32. Baltus AE, Menke DB, Hu YC, Goodheart ML, Carpenter AE, de Rooij DG, Page DC (2006) In germ cells of mouse embryonic ovaries, the decision to enter meiosis precedes premeiotic DNA replication. Nat Genet 38(12):1430–1434. https://doi.org/10.1038/ng1919
33. Koubova J, Menke DB, Zhou Q, Capel B, Griswold MD, Page DC (2006) Retinoic acid regulates sex-specific timing of meiotic initiation in mice. Proc Natl Acad Sci USA 103(8):2474–2479. https://doi.org/10.1073/pnas.0510813103
34. Kocer A, Reichmann J, Best D, Adams IR (2009) Germ cell sex determination in mammals. Mol Hum Reprod 15(4):205–213. https://doi.org/10.1093/molehr/gap008
35. Haston KM, Tung JY, Reijo Pera RA (2009) Dazl functions in maintenance of pluripotency and genetic and epigenetic programs of differentiation in mouse primordial germ cells in vivo and in vitro. PLoS One 4(5):e5654. https://doi.org/10.1371/journal.pone.0005654
36. Woods DC, Tilly JL (2013) Isolation, characterization and propagation of mitotically active germ cells from adult mouse and

human ovaries. Nat Protoc 8(5):966–988. https://doi.org/10.1038/nprot.2013.047
37. McLaren A (2000) Germ and somatic cell lineages in the developing gonad. Mol Cell Endocrinol 163(1–2):3–9. https://doi.org/10.1016/s0303-7207(99)00234-8
38. Jameson SA, Natarajan A, Cool J, DeFalco T, Maatouk DM, Mork L, Munger SC, Capel B (2012) Temporal transcriptional profiling of somatic and germ cells reveals biased lineage priming of sexual fate in the fetal mouse gonad. PLoS Genet 8(3):e1002575. https://doi.org/10.1371/journal.pgen.1002575
39. Mazaud S, Oreal E, Guigon CJ, Carre-Eusebe D, Magre S (2002) Lhx9 expression during gonadal morphogenesis as related to the state of cell differentiation. Gene Expr Patterns GEP 2(3–4):373–377. https://doi.org/10.1016/s1567-133x(02)00050-9
40. Kanamori-Katayama M, Kaiho A, Ishizu Y, Okamura-Oho Y, Hino O, Abe M, Kishimoto T, Sekihara H, Nakamura Y, Suzuki H, Forrest AR, Hayashizaki Y (2011) LRRN4 and UPK3B are markers of primary mesothelial cells. PLoS One 6(10):e25391. https://doi.org/10.1371/journal.pone.0025391
41. Piprek RP, Kolasa M, Podkowa D, Kloc M, Kubiak JZ (2018) Transcriptional profiling validates involvement of extracellular matrix and proteinases genes in mouse gonad development. Mech Dev 149:9–19. https://doi.org/10.1016/j.mod.2017.11.001
42. Brennan J, Karl J, Capel B (2002) Divergent vascular mechanisms downstream of Sry establish the arterial system in the XY gonad. Dev Biol 244(2):418–428. https://doi.org/10.1006/dbio.2002.0578
43. Jeays-Ward K, Hoyle C, Brennan J, Dandonneau M, Alldus G, Capel B, Swain A (2003) Endothelial and steroidogenic cell migration are regulated by WNT4 in the developing mammalian gonad. Development 130(16):3663–3670. https://doi.org/10.1242/dev.00591
44. Lummertz da Rocha E, Rowe RG, Lundin V, Malleshaiah M, Jha DK, Rambo CR, Li H, North TE, Collins JJ, Daley GQ (2018) Reconstruction of complex single-cell trajectories using CellRouter. Nat Commun 9(1):892. https://doi.org/10.1038/s41467-018-03214-y
45. Harigae H, Nakajima O, Suwabe N, Yokoyama H, Furuyama K, Sasaki T, Kaku M, Yamamoto M, Sassa S (2003) Aberrant iron accumulation and oxidized status of erythroid-specific delta-aminolevulinate synthase (ALAS2)-deficient definitive erythroblasts. Blood 101(3):1188–1193. https://doi.org/10.1182/blood-2002-01-0309
46. de Jong J, Stoop H, Gillis AJ, van Gurp RJ, van de Geijn GJ, Boer M, Hersmus R, Saunders PT, Anderson RA, Oosterhuis JW, Looijenga LH (2008) Differential expression of SOX17 and SOX2 in germ cells and stem cells has biological and clinical implications. J Pathol 215(1):21–30. https://doi.org/10.1002/path.2332
47. Ohta H, Kurimoto K, Okamoto I, Nakamura T, Yabuta Y, Miyauchi H, Yamamoto T, Okuno Y, Hagiwara M, Shirane K, Sasaki H, Saitou M (2017) In vitro expansion of mouse primordial germ cell-like cells recapitulates an epigenetic blank slate. EMBO J 36(13):1888–1907. https://doi.org/10.15252/embj.201695862
48. Malki S, van der Heijden GW, O'Donnell KA, Martin SL, Bortvin A (2014) A role for retrotransposon LINE-1 in fetal oocyte attrition in mice. Dev Cell 29(5):521–533. https://doi.org/10.1016/j.devcel.2014.04.027
49. Morohaku K, Tanimoto R, Sasaki K, Kawahara-Miki R, Kono T, Hayashi K, Hirao Y, Obata Y (2016) Complete in vitro generation of fertile oocytes from mouse primordial germ cells. Proc Natl Acad Sci USA 113(32):9021–9026. https://doi.org/10.1073/pnas.1603817113
50. Watanabe Y, Nurse P (1999) Cohesin Rec8 is required for reductional chromosome segregation at meiosis. Nature 400(6743):461–464. https://doi.org/10.1038/22774
51. De Felici M, Farini D (2012) The control of cell cycle in mouse primordial germ cells: old and new players. Curr Pharm Des 18(3):233–244. https://doi.org/10.2174/138161212799040448
52. Xu H, Beasley MD, Warren WD, van der Horst GT, McKay MJ (2005) Absence of mouse REC8 cohesin promotes synapsis of sister chromatids in meiosis. Dev Cell 8(6):949–961. https://doi.org/10.1016/j.devcel.2005.03.018
53. Zhou H, Grubisic I, Zheng K, He Y, Wang PJ, Kaplan T, Tjian R (2013) Taf7l cooperates with Trf2 to regulate spermiogenesis. Proc Natl Acad Sci USA 110(42):16886–16891. https://doi.org/10.1073/pnas.1317034110
54. Yang F, Eckardt S, Leu NA, McLaughlin KJ, Wang PJ (2008) Mouse TEX15 is essential for DNA double-strand break repair and chromosomal synapsis during male meiosis. J Cell Biol 180(4):673–679. https://doi.org/10.1083/jcb.200709057
55. Tsukamoto H, Yoshitake H, Mori M, Yanagida M, Takamori K, Ogawa H, Takizawa T, Araki Y (2006) Testicular proteins associated with the germ cell-marker, TEX101: involvement of cellubrevin in TEX101-trafficking to the cell surface during spermatogenesis. Biochem Biophys Res Commun 345(1):229–238. https://doi.org/10.1016/j.bbrc.2006.04.070
56. Baudat F, Buard J, Grey C, Fledel-Alon A, Ober C, Przeworski M, Coop G, de Massy B (2010) PRDM9 is a major determinant of meiotic recombination hotspots in humans and mice. Science 327(5967):836–840. https://doi.org/10.1126/science.1183439
57. Zhou J, Leu NA, Eckardt S, McLaughlin KJ, Wang PJ (2014) STK31/TDRD8, a germ cell-specific factor, is dispensable for reproduction in mice. PLoS One 9(2):e89471. https://doi.org/10.1371/journal.pone.0089471
58. Akagi T, Kuure S, Uranishi K, Koide H, Costantini F, Yokota T (2015) ETS-related transcription factors ETV4 and ETV5 are involved in proliferation and induction of differentiation-associated genes in embryonic stem (ES) cells. J Biol Chem 290(37):22460–22473. https://doi.org/10.1074/jbc.M115.675595
59. Atienza JM, Roth RB, Rosette C, Smylie KJ, Kammerer S, Rehbock J, Ekblom J, Denissenko MF (2005) Suppression of RAD21 gene expression decreases cell growth and enhances cytotoxicity of etoposide and bleomycin in human breast cancer cells. Mol Cancer Ther 4(3):361–368. https://doi.org/10.1158/1535-7163.MCT-04-0241
60. Zhang D, Wang Y, Lu P, Wang P, Yuan X, Yan J, Cai C, Chang CP, Zheng D, Wu B, Zhou B (2017) REST regulates the cell cycle for cardiac development and regeneration. Nat Commun 8(1):1979. https://doi.org/10.1038/s41467-017-02210-y
61. Yamaguchi S, Kimura H, Tada M, Nakatsuji N, Tada T (2005) Nanog expression in mouse germ cell development. Gene Expr patterns GEP 5(5):639–646. https://doi.org/10.1016/j.modgep.2005.03.001
62. Loenarz C, Ge W, Coleman ML, Rose NR, Cooper CD, Klose RJ, Ratcliffe PJ, Schofield CJ (2010) PHF8, a gene associated with cleft lip/palate and mental retardation, encodes for an Nepsilon-dimethyl lysine demethylase. Hum Mol Genet 19(2):217–222. https://doi.org/10.1093/hmg/ddp480
63. Metcalf CE, Wassarman DA (2007) Nucleolar colocalization of TAF1 and testis-specific TAFs during Drosophila spermatogenesis. Dev Dyn 236(10):2836–2843. https://doi.org/10.1002/dvdy.21294
64. Zabludoff SD, Wright WW, Harshman K, Wold BJ (1996) BRCA1 mRNA is expressed highly during meiosis and spermiogenesis but not during mitosis of male germ cells. Oncogene 13(3):649–653
65. Wilkinson DA, Neale GA, Mao S, Naeve CW, Goorha RM (1997) Elf-2, a rhombotin-2 binding ets transcription factor: discovery and potential role in T cell leukemia. Leukemia 11(1):86–96. https://doi.org/10.1038/sj.leu.2400516
66. Varaljai R, Islam AB, Beshiri ML, Rehman J, Lopez-Bigas N, Benevolenskaya EV (2015) Increased mitochondrial function

downstream from KDM5A histone demethylase rescues differentiation in pRB-deficient cells. Genes Dev 29(17):1817–1834. https://doi.org/10.1101/gad.264036.115
67. Palma-Gudiel H, Cordova-Palomera A, Leza JC, Fananas L (2015) Glucocorticoid receptor gene (NR3C1) methylation processes as mediators of early adversity in stress-related disorders causality: a critical review. Neurosci Biobehav Rev 55:520–535. https://doi.org/10.1016/j.neubiorev.2015.05.016
68. Wang L, Jiang Z, Huang D, Duan J, Huang C, Sullivan S, Vali K, Yin Y, Zhang M, Wegrzyn J, Tian XC, Tang Y (2018) JAK/STAT3 regulated global gene expression dynamics during late-stage reprogramming process. BMC Genom 19(1):183. https://doi.org/10.1186/s12864-018-4507-2
69. Qiu X, Mao Q, Tang Y, Wang L, Chawla R, Pliner HA, Trapnell C (2017) Reversed graph embedding resolves complex single-cell trajectories. Nat Methods 14(10):979–982. https://doi.org/10.1038/nmeth.4402
70. Okashita N, Suwa Y, Nishimura O, Sakashita N, Kadota M, Nagamatsu G, Kawaguchi M, Kashida H, Nakajima A, Tachibana M, Seki Y (2016) PRDM14 drives OCT3/4 recruitment via active demethylation in the transition from primed to naive pluripotency. Stem cell Rep 7(6):1072–1086. https://doi.org/10.1016/j.stemcr.2016.10.007
71. Thomas FH, Vanderhyden BC (2006) Oocyte-granulosa cell interactions during mouse follicular development: regulation of kit ligand expression and its role in oocyte growth. Reprod Biol Endocrinol RB&E 4:19. https://doi.org/10.1186/1477-7827-4-19
72. Liu S, Trapnell C (2016) Single-cell transcriptome sequencing: recent advances and remaining challenges. F1000Res. https://doi.org/10.12688/f1000research.7223.1
73. Bacher R, Kendziorski C (2016) Design and computational analysis of single-cell RNA-sequencing experiments. Genome Biol 17:63. https://doi.org/10.1186/s13059-016-0927-y
74. Rheaume BA, Jereen A, Bolisetty M, Sajid MS, Yang Y, Renna K, Sun L, Robson P, Trakhtenberg EF (2018) Author Correction: single cell transcriptome profiling of retinal ganglion cells identifies cellular subtypes. Nat Commun 9(1):3203. https://doi.org/10.1038/s41467-018-05792-3
75. Li L, Dong J, Yan L, Yong J, Liu X, Hu Y, Fan X, Wu X, Guo H, Wang X, Zhu X, Li R, Yan J, Wei Y, Zhao Y, Wang W, Ren Y, Yuan P, Yan Z, Hu B, Guo F, Wen L, Tang F, Qiao J (2017) Single-cell RNA-seq analysis maps development of human germline cells and gonadal niche interactions. Cell Stem Cell 20(6):891–892. https://doi.org/10.1016/j.stem.2017.05.009
76. Kalkan T, Bornelov S, Mulas C, Diamanti E, Lohoff T, Ralser M, Middelkamp S, Lombard P, Nichols J, Smith A (2019) Complementary activity of ETV5, RBPJ, and TCF3 drives formative transition from naive pluripotency. Cell Stem Cell. https://doi.org/10.1016/j.stem.2019.03.017
77. Nicholas CR, Chavez SL, Baker VL, Reijo Pera RA (2009) Instructing an embryonic stem cell-derived oocyte fate: lessons from endogenous oogenesis. Endocr Rev 30(3):264–283. https://doi.org/10.1210/er.2008-0034